Response to RC2

We sincerely thank the reviewer #2 for the constructive and detailed review of our manuscript. We appreciate the positive overall assessment and the valuable suggestions that have helped us improve the clarity, precision, and scientific rigor of the work. In particular, we have strengthened the description of the historical validation for the 2010 period, adopted more precise temporal terminology throughout, expanded the discussion on the physical interpretation and limitations of the map with respect to permafrost depth, and clarified the transferability of the methodology. All comments have been carefully addressed in the revised manuscript.

Below, the reviewer's original comments are shown in **blue**, our responses are given in **black**, and the corresponding revisions added to the main text are highlighted in **red**.

Chen et al. present a 1x1 km map of permafrost conditions on the Qinghai–Tibet Plateau for the 2020 period, along with a novel methodology for deriving said map without access to extensive field data for this period. The authors also perform extensive validation of their methodology and output against available observational data and permafrost maps. I applaud Chen et al. for including the MLP model despite its deficiencies, which can help guide similar applications in the future. Overall, my judgement is that this study is well suited for publication in The Cryosphere.

Response: We sincerely thank the reviewer for the positive assessment and for the thoughtful comments that helped us improve the manuscript. We have revised the text to more clearly present the historical validation of the methodology on the 2010 data, adopted consistent and precise temporal language ("2020 period"), strengthened the discussion of map limitations with respect to permafrost depth, and expanded the section on methodological transferability. Our point-by-point responses are provided below.

Specific comments:

1. How well does the presented methodology for estimating the soil parameter E perform for the 2010 period? If I understand correctly, the authors compare estimated E for 2020 period to the E **determined from the field surveys in 2010.** It would be interesting to see how well the two methods are in estimating E for 2010, and how the estimated E has changed from 2010 period to the 2020 period.

Response: We thank the reviewer for this important question. This validation is already presented in the manuscript. Table 1 reports the accuracy of four sampling strategies when the Random Forest model (trained on environmental covariates) is used to reproduce the benchmark *E* field derived from field surveys in Cao et al. (2023) for the 2010 period. The optimal configuration (*k*-means

sampling with 5000 points) achieves a correlation coefficient of r = 0.862, RMSE = 0.048, and explains 74.83% of the spatial variance in the 2010 *E* values. These metrics demonstrate that the methodology can reliably reconstruct the 2010 *E* field from environmental drivers.

To make this historical validation more immediately visible to readers, we have revised the caption of Table 1 as follows:

Table 1 Comparison of the predictive accuracy of four sampling strategies for estimating the local soil parameter *E* for the 2010 period. The benchmark parameter *E* used for validation was derived from extensive field surveys and the Clustering-Optimization-Prediction procedure in Cao et al. (2023). Accuracy metrics (RMSE, MAE, *r*, and % variance explained) are derived from 5-fold cross-validation using an optimal sample size of 5000 points.

Sampling method	RMSE	MAE	r	% variance explained
k-means sampling	0.048	0.029	0.862	74.83
Equal Range (ER) sampling	0.049	0.030	0.831	69.18
PCA-based sampling	0.049	0.030	0.831	69.90
Latin Hypercube Sampling (LHS)	0.054	0.036	0.806	65.74

We have also clarified the description in Section 3.3 and revised the caption of Figure 4 to explicitly distinguish the 2010 *E* field (from Cao et al., 2023) from the 2020-period *E* field predicted using the space-for-time approach. The decadal changes in *E* (Figure 4c) are therefore derived from two independently generated fields rather than from applying the new method to both periods.

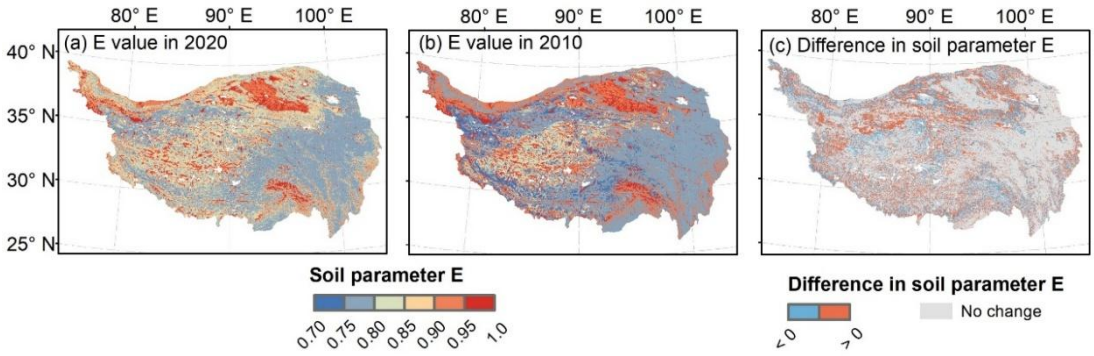

Figure R1 (Figure 4 in the revised manuscript) Spatial distribution of the soil parameter E in the 2020 period (a) and the 2010 period (b). (c) illustrates the difference (2020 minus 2010), where positive values (red) indicate an increase in E (conditions conducive to degradation) and negative values (blue) indicate a decrease. The 2010 E map was derived from Cao et al. (2023), whereas the 2020 E map was predicted using a space-for-time substitution strategy that transferred the statistical relationships established in the 2020 period between E and its environmental drivers.

2.The authors consistently refer to the permafrost distribution being for 2020, while in they are using data aggregated over 5 years to predict this distribution. Moreover, regions are classified as seasonally frozen ground if conditions are unfavourable for permafrost during this temporal period, while it can take substantially longer for deep permafrost to completely disappear. I would thus encourage a more precise language regarding the time of validity of the map, and how the classifications relate to the transient thermal state of the ground.

Response: We thank the reviewer for the rigorous and important comment. We have revised the manuscript throughout to consistently use the term "2020 period" instead of "2020" or "instantaneous snapshot." This better reflects that the thermal forcing indices and environmental covariates are averaged over the 2016–2020 period.

Regarding the deeper concern about permafrost depth and transience, we have added the following clarification in the Discussion section:

"Despite its robustness, the methodology remains subject to certain limitations. First, the permafrost distribution map primarily reflects the thermal state of the near-surface ground, at depths of roughly 10-15 meters. It cannot resolve deep paleopermafrost (relict permafrost) that lies below the depth of zero annual amplitude. Consequently, areas classified as SFG in the 2020-period map may still contain relict permafrost at greater depths that has not yet fully responded to recent warming. The map should therefore be interpreted as indicating the current thermal state of the upper permafrost layer rather than the complete disappearance of permafrost at all depths. In the central QTP transition zones, where ground temperatures at 10–15 m depth were already close to 0 °C around 2010, the shift from permafrost to SFG conditions within a decade is physically plausible and consistent with borehole observations."

3. I would welcome a discussion on the transferability of the presented mapping approach to other climates/environments. It would be interesting to hear the authors thoughts on which aspects of the method, including assumptions, are generalizable, and which are specific to the context of the Qinghai–Tibet Plateau

Response: We thank the reviewer for this valuable suggestion. We have added a dedicated paragraph in the Discussion section addressing the transferability of the methodology.

The added text reads:

"In principle, the overall mapping methodology is transferable to other permafrost environments, such as the Mongolian Plateau or parts of the Arctic. However, successful application requires a locally calibrated parameter E that reflects regional environmental conditions. The statistical relationships derived for the QTP cannot be directly transferred. High-quality field survey data from the target region are therefore needed to establish the benchmark E field for at least one period. In

addition, the correction of satellite-derived thawing indices must be adapted to local conditions. The multiple linear regression model used here (based on LST-derived DDT, NDVI and latitude) was optimized for the QTP, where winter snow cover is generally thin and ephemeral. In regions with thick, persistent snow cover (e.g., much of Arctic Russia or boreal Canada), an explicit snow insulation term would be required when calculating the freezing index. The space-for-time substitution strategy itself is conceptually generalizable, provided the assumption of approximate stationarity in driver–*E* relationships holds over the extrapolation interval, which should be evaluated on a case-by-case basis."

Technical comments:

Line 56-62: This paragraph warrants some reference(s), e.g. for the mentioned "previous mapping efforts" or for the applications requiring "year-specific benchmarks"

Response: We have added appropriate references (Obu et al. 2019, Zou et al. 2017; Ran et al., 2012; Cao et al. 2023; Ran et al. 2021) to support the statements regarding previous mapping efforts and the need for year-specific maps.

Line 97: please use "per decade" rather than "/10a"

Response： Accepted.

Line 162-163: This does not fit to the subsection "Existing permafrost datasets for comparison", please move or revise header.

Response： We thank the reviewer for catching this inconsistency. We have removed the two sentences from this subsection. Glacier extent data (Ye et al., 2017) and 2020 lake boundaries (Zhang et al., 2021) are now introduced in Section 2.1 (Study area) and are also mentioned in the caption of Figure 6.

Section 4.1: It would be interesting to know if there is also a temporal trend in DDT_{LST}, or if the presented cooling pattern is only present in the corrected DDT_{GST} values.

Response: We thank the reviewer for this suggestion. We have added a new supplementary figure (Figure R2 in the response letter) comparing the spatial patterns and decadal changes of DDT_{LST} and DDT_{GST}.

The results show that the eastern cooling signal is present in both (Figure R2), but becomes clearer and more spatially coherent after the vegetation and latitude correction. In the Three-River Headwater region outlined by the blue box in Figure R2f, the central area exhibits slight warming and cooling signals, with the positive and negative changes generally within ±5%, relative to 2000 °C·d. The cooling signal is more pronounced in the eastern part of the plateau, where the decrease in DDT in most areas ranges between 5% and 15%.

To further validate the DDT_{GST} cooling signal in the eastern region, we compared observations from 8 meteorological stations (as indicated in Figure R2f), among which 6 stations showed a clear decreasing trend in DDT, confirming the eastern cooling trend shown in the map.

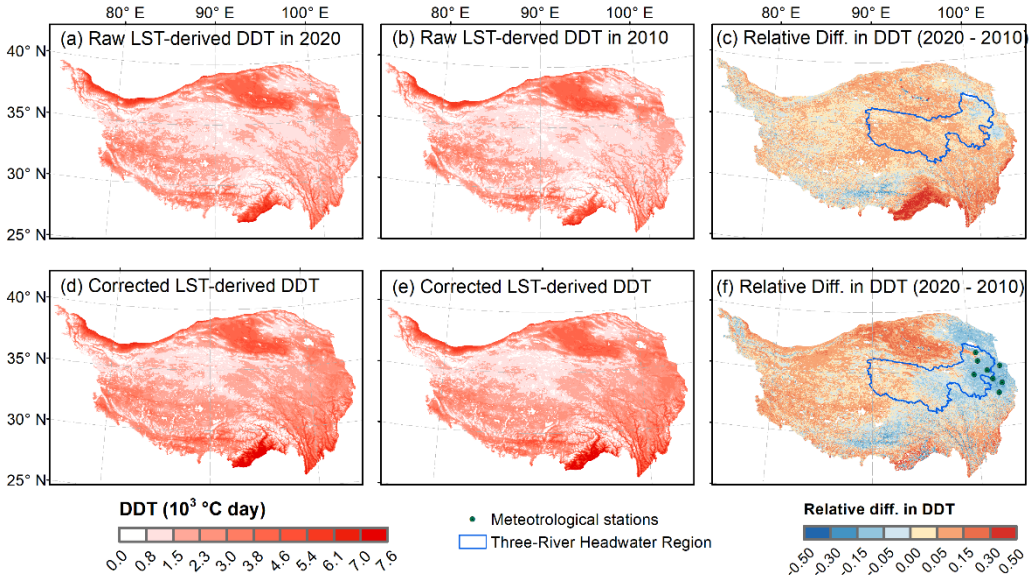

Figure R2 Spatial distribution and decadal of thawing indices (DDT) on the QTP. (a-c) display the LST-derived DDT and its relative changes, (d-f) displays the corrected DDT and its relative changes.

We have also revised panels (c) and (f) of Figure 3 (Figure R3 in this letter) to show relative differences for better interpretability of decadal changes.

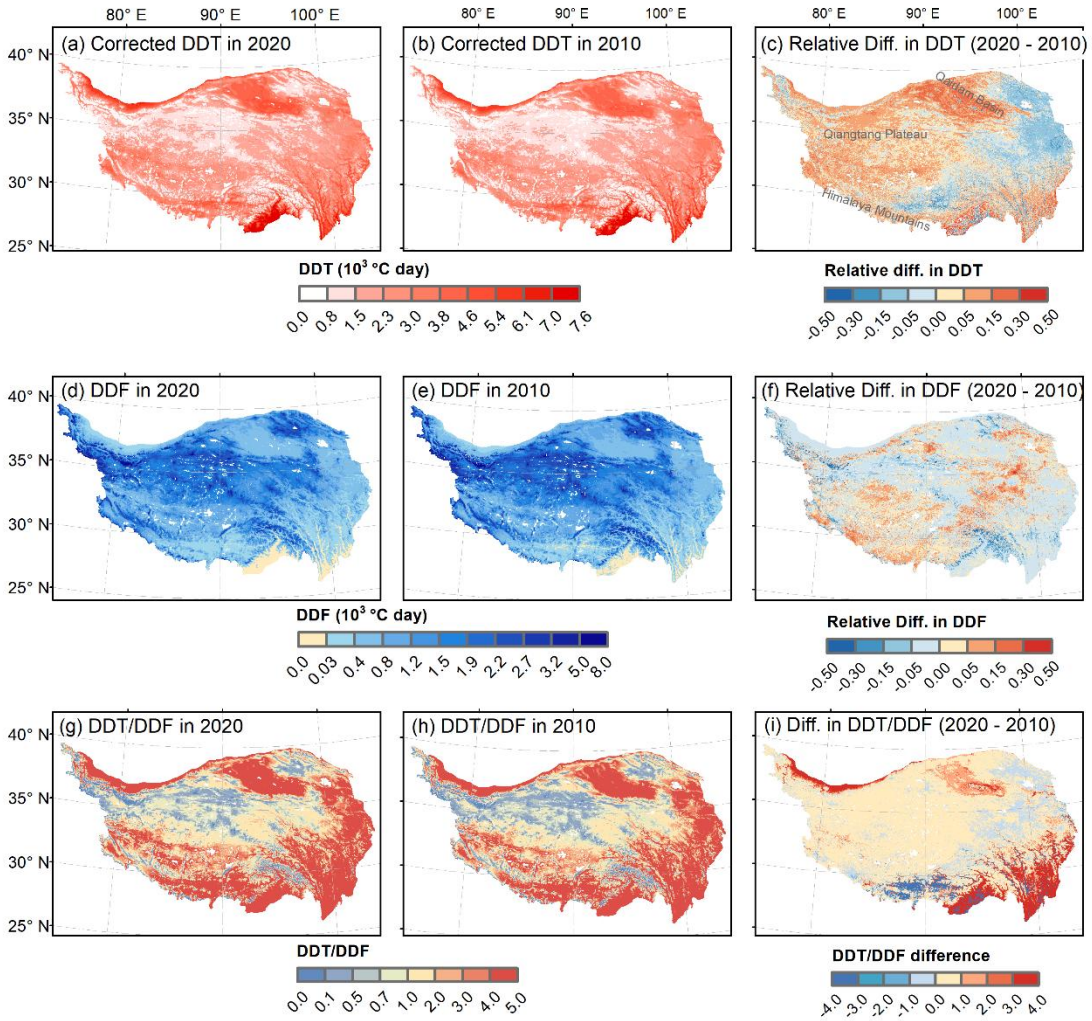

Figure R3 (Figure 3 in the revised manuscript) Spatial distribution and decadal changes of thermal forcing indices on the QTP. (a-c) displays the ground surface thawing index and its relative changes, (d-f) the freezing index and its relative changes. (g-i) the ratio of thawing to freezing indices and its decadal change. The left and middle columns present the spatial distribution for the 2020 and 2010 periods, respectively. The right column shows the decadal differences between 2020 and 2010 periods. Notably, the relative differences in (c) and (f) are calculated using baseline denominators of 2000 °C·d and 1200 °C·d, respectively, which are determined based on the regional mean values of DDT and DDF averaged across the 2010 and 2020 periods. For (c) and (i), positive values (red) indicate warming/instability, while negative values (blue) indicate cooling/stability. For (f), negative values (red) indicate winter warming (reduced freezing), while positive values (blue) indicate cooling.

Line 294: Please indicate on this or the overview map where the “southern Himalayan margin” is.

Response: Accepted. We have updated Figure 1 (Figure R4 in this letter) to include major geographic features, including the Himalaya Mountains, and have added boundaries for the Three-River Headwater Region and the locations of validation boreholes.

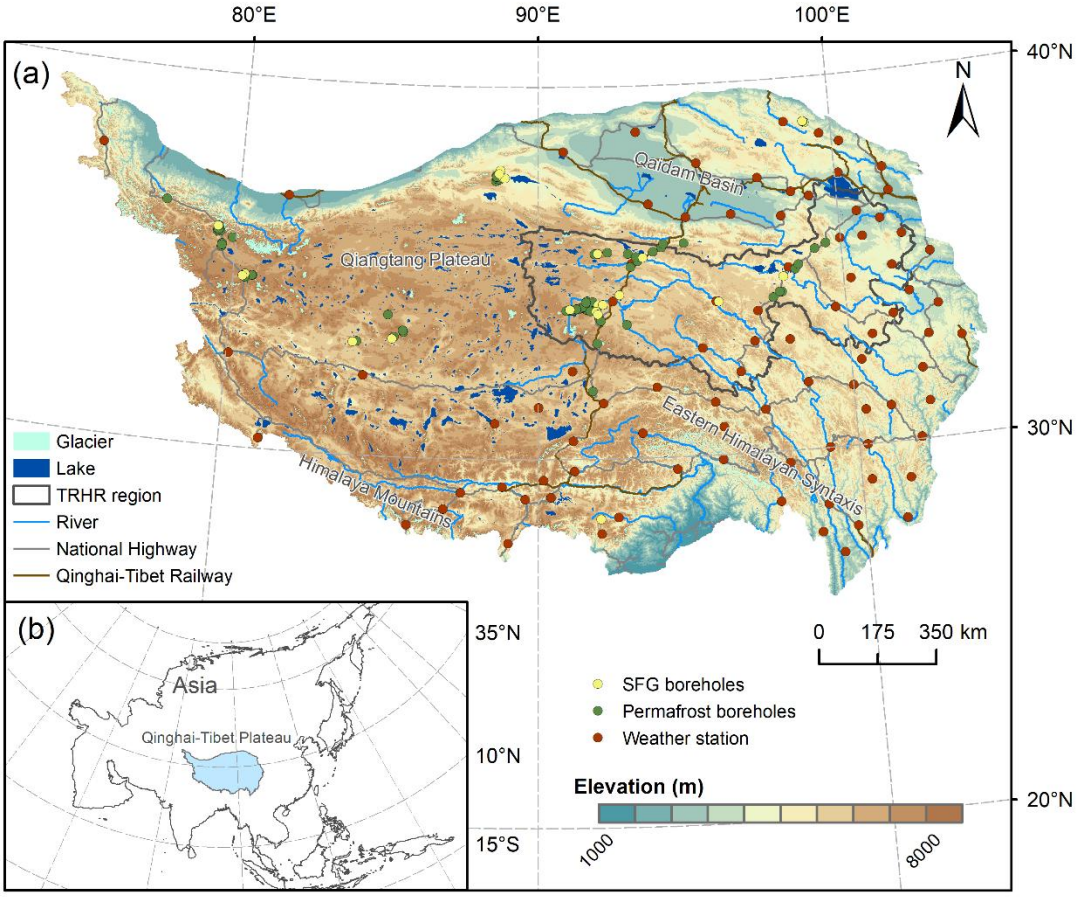

Figure R4 Topographic map and geographical context of the Qinghai-Tibet Plateau (QTP). (a) The topography of the region. The background color gradient represents elevation derived from the Shuttle Radar Topography Mission DEM. The 87 national meteorological stations (red dots) used for ground surface temperature correction, alongside major river systems and lakes are shown. Notably, the 83 permafrost boreholes and 26 seasonally frozen ground (SFG) boreholes for validation are primarily distributed within the Three-River Headwater Region (TRHR). (b) The location of the QTP in Asia.

Line 306: Do you mean “temporally extrapolate”?

Response: Yes, this was a typographical error. We have corrected it in the revised manuscript.

Figure 4: It is not clear to me if the “E value in 2010” refers to the values from Cao et al. (2023). Please be specific here and elsewhere in the manuscript whether the “E values” and “Permafrost maps” from 2010 refer to the original Cao et al. publication or if they refer to your estimated E values and the thereof calculated permafrost maps.

Response: We have revised the caption of Figure 4 and the relevant text in Section 3.3 and Section

4.2 to explicitly state that the 2010 *E* field was derived from Cao et al. (2023), while the 2020-period *E* field was predicted using the space-for-time substitution strategy.

Line 366: It's unclear to me where the "Three-River Headwater Region" is. Please include the placenames used in the text in the relevant figure of in the overview map in Figure 1.

Response: We have updated Figure 1 to clearly delineate the Three-River Headwater Region.

Line 407: You state that you identify "four out of five confirmed SFG boreholes", but there appears to be eight purple "borehole with seasonal frost" markers in Figure 8c.

Response: We thank the reviewer for catching this inconsistency. We have redrawn Figure 7 (and Figure 8) with improved symbology and have ensured that the grey dashed boxes and borehole counts are consistent with the text. The revised figures now clearly show five SFG boreholes within the focused subregion.

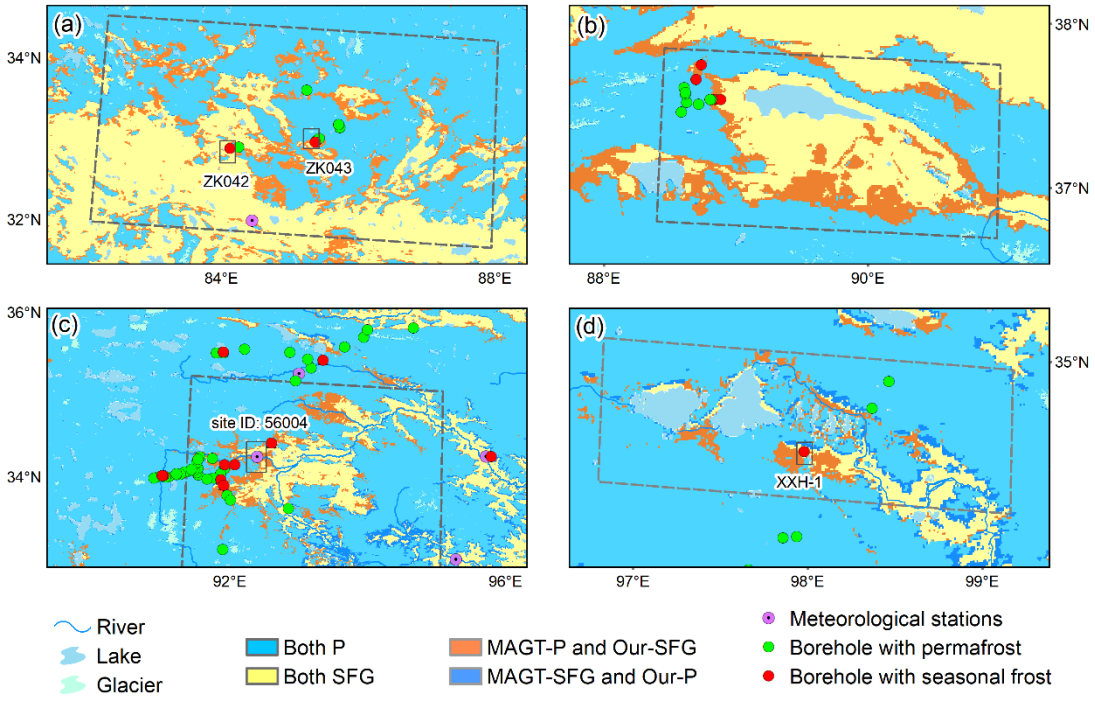

Figure R5 (Figure 7 in the revised manuscript) Detailed validation of spatial inconsistencies between the generated 2020 map and the MAGT-based map using ground-truth observations. The panels (a)-(d) correspond to the four subregions outlined in Fig. 7a. "MAGT-P and Our-SFG" represents regions classified as permafrost by the MAGT-based map but as SFG by our map. "MAGT-SFG and Our-P" indicates the opposite.

Figure 8 & 9: I find it hard to distinguish the borehole markers, please consider revising the symbols for readability.

Response: Both figures have been redrawn with larger, more distinct symbols for better readability.

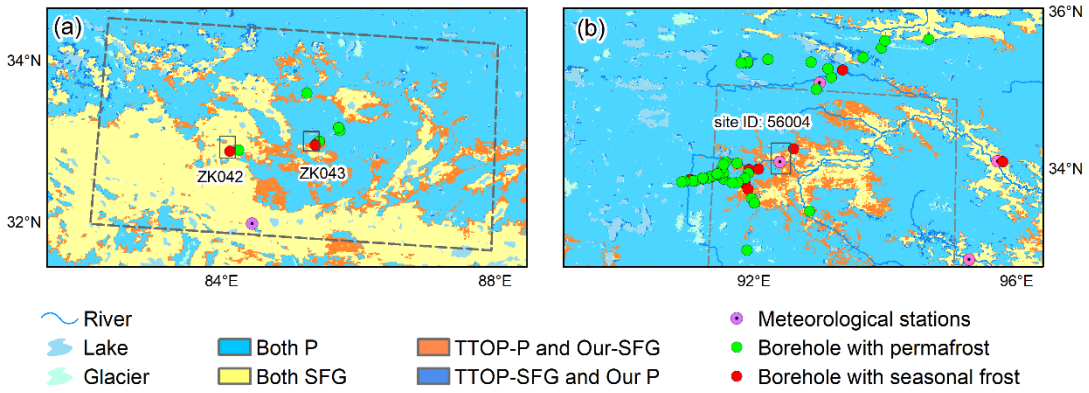

Figure R6 (Figure 8 in the revised manuscript) Detailed validation of spatial inconsistencies between the generated 2020 map and the TTOP-based map in two key transition zones. Panels (a) and (b) correspond to the subregions (a and c) outlined in Fig. 7b. "TTOP-P and Our-SFG" indicates areas identified as permafrost by the TTOP-based map but as SFG by our map. "TTOP-SFG and Our-P" indicates the opposite.

Line 446: it is unclear where the classifications "continuous and discontinuous permafrost" come from, and if they are relevant for this context.

Response: We have removed the terms "continuous" and "discontinuous permafrost" from the manuscript and now refer to the "transition zone between permafrost and SFG in the plateau hinterland."

Line 466: Where do the datasets of thermokarst lakes and engineering instabilities come from? Remote sensing, field mapping?

Response: We have added the data sources in both the main text and the caption of Figure 11: thermokarst lakes were extracted from Sentinel-2A imagery by Chen et al. (2021), and engineering defect points were obtained from field surveys compiled by Li (2021).

"The spatial pattern of our simulated degradation exhibits a strong correspondence with the distribution of thermokarst lakes identified from Sentinel-2A imagery (Chen et al., 2021) and known engineering defect points (Li, 2021) along the Qinghai-Tibet Railway and Highway (Fig. 11a)."

"Figure 11 Distribution and changes of frozen ground types in two degradation hotspots on the QTP from 2010 to 2020 periods. Panels (a) and (b) corresponds to subregions (a) and (b) in Fig. 9, respectively. (a) Changes in the central QTP, where the dominant transition is from permafrost to SFG. Thermokarst lakes (extracted from Sentinel-2A imagery) (Chen et al., 2021) and engineering defect points (mapped via manual field surveys) (Li, 2021) are superimposed on the map to serve as proxies for permafrost instability. (b) Changes in the southern QTP, characterized by the transition from SFG to non-frozen ground. The observed 0cm GST values from two meteorological stations (ID: 56533, 56548) provide validation for the model results."

References:

[1] Chen, X., Mu, C., Jia, L., Li, Z., Fan, C., Mu, M., Peng, X., Wu, X. (2021). Thermokarst lakes on the Qinghai-Tibet Plateau (2018). Third Pole Environment Data Center. https://doi.org/10.11888/Geocry.tpdc.271205.

[2] Li, G. (2021). Survey data of major frozen soil engineering diseases in South Asia channel and Himalayas (2020-2021). Third Pole Environment Data Center. https://doi.org/10.11888/Cryos.tpdc.271880.

Line 492-502 and elsewhere: I'm surprised that so much attention is given to the transition of seasonally frozen ground to non-frozen ground. While this is an interesting transition, I think this can be deemphasized as the manuscript is about permafrost mapping.

Response: We agree with the reviewer's assessment. We have substantially condensed and refocused this discussion to maintain emphasis on permafrost dynamics, while retaining only the essential validation from the two meteorological stations.

"In contrast, the degradation pattern in the southern QTP (Fig. 11b) was characterized by the contraction of the frozen ground range, manifested as the conversion of SFG to non-frozen ground. Ground-truth validation from meteorological stations 56533 and 56548 confirms this transition: observed records from 2016 to 2019 show a freezing index of zero, indicating the complete absence of ground freezing throughout the year (Fig. 11b). Compared with the central QTP, degradation in this region were primarily associated with enhanced summer warming, as the increase in DDT within degraded areas was more than twice than that observed in adjacent stable SFG regions (Fig. 13a). This processed was further accompanied by an increase in the soil parameter E (Fig. 13d), which likely accelerated the disappearance of SFG."